JMI Journal of Medical Imaging

RESEARCH PAPER

Accelerated parallel magnetic resonance imaging with compressed sensing using structured sparsity

Nicholas Dwork,[a,b,*] **Jeremy W. Gordon**,[c] **and Erin K. Englund**[b]

[a]University of Colorado—Anschutz Medical Campus, Department of Biomedical Informatics, Aurora, Colorado, United States

[b]University of Colorado—Anschutz Medical Campus, Department of Radiology, Aurora, Colorado, United States

[c]University of San Francisco California, Department of Radiology and Biomedical Imaging, San Francisco, California, United States

ABSTRACT. **Purpose:** We present a method that combines compressed sensing with parallel imaging that takes advantage of the structure of the sparsifying transformation.

Approach: Previous work has combined compressed sensing with parallel imaging using model-based reconstruction but without taking advantage of the structured sparsity. Blurry images for each coil are reconstructed from the fully sampled center region. The optimization problem of compressed sensing is modified to take these blurry images into account, and it is solved to estimate the missing details.

Results: Using data of brain, ankle, and shoulder anatomies, the combination of compressed sensing with structured sparsity and parallel imaging reconstructs an image with a lower relative error than does sparse SENSE or L1 ESPIRiT, which do not use structured sparsity.

Conclusions: Taking advantage of structured sparsity improves the image quality for a given amount of data as long as a fully sampled region centered on the zero frequency of the appropriate size is acquired.

 [DOI: 10.1117/1.JMI.11.3.033504]

Keywords: magnetic resonance imaging; structured sparsity; compressed sensing; parallel imaging

Paper 23343GR received Nov. 21, 2023; revised Apr. 25, 2024; accepted Jun. 3, 2024; published Jun. 26, 2024.

1 Introduction

Magnetic resonance imaging (MRI) is a ubiquitously used gross imaging modality due to its ability to image with significant natural contrast (without any exogenous contrast agent) and its complete lack of ionizing radiation. MRI acquires samples in the frequency domain. With a fully sampled reconstruction, sufficient data are acquired to satisfy the Nyquist–Shannon sampling theorem, and the image is reconstructed with a simple inverse fast Fourier transform. Because MRI requires that the patient remains still during the scan, acquiring this amount of data is especially challenging for three-dimensional (3D) MRI, which requires scan times up to 10 min for conventional reconstruction. Two methods of accelerating MRI include parallel imaging and compressed sensing. Parallel imaging uses multiple sensing coils (i.e., antennas) to simultaneously image the subject from different vantage points.[1,2] The unique information

*Address all correspondence to Nicholas Dwork, nicholas.dwork@cuanschutz.edu

2329-4302/2024/$28.00

provided by each antenna can be used to interpolate missing Fourier values and reconstruct a high-quality image. Compressed sensing relies on the knowledge that the image is sparse after a sparsifying transformation. With combinations of these methods, MRI requires even fewer samples for a high-quality image, which can be collected with an even faster scan.

3D MRI with compressed sensing and parallel imaging still requires ~30 s of scan time.[3] Although this is much faster than the conventional fully sampled acquisition, any further increase in speed could make MRI even more robust to motion or increase patient throughput. In previous work, we showed that compressed sensing could be accelerated with structured sparsity.[4,5] The sparsifying transformations used with compressed sensing are commonly the wavelet[6,7] and/or curvelet[8] transforms, which benefit from fast implementations.[9,10] Both the wavelet and curvelet transforms apply a low-pass filter to the image; most natural images, and certainly anatomical MR images, have high energy in the low frequencies. Thus, one would not expect the intensities of the coefficients corresponding to these low frequencies to be sparse. In Refs. 4 and 5, Dwork et al. modified the standard optimization problem solved for a compressed sensing reconstruction to take this into account. By doing so, they generated images of higher quality for a given number of samples.

In this work, we combine model-based parallel imaging[11] with compressed sensing using structured sparsity, and we show that we can recover high-quality images with MRI using even fewer samples, which can be collected with a faster scan.

2 Methods

2.1 Background

With parallel MRI, multiple sensing coils are used to simultaneously collect data of a patient. With model-based reconstruction, it is assumed that the sensitivity of each coil is known, which specifies how well the coil senses from each point in space. The image is reconstructed by solving the following least squares problem:

$$\underset{x}{\text{minimize}} \ \|\mathbf{MFS}x - \mathbf{b}\|_2, \tag{1}$$

where x represents the image, $\|\cdot\|_2$ represents the ℓ_2 norm, $\mathbf{S}$ is a block-column matrix such that $\mathbf{S} = (S^{(1)}, S^{(2)}, \ldots, S^{(C)})$, $S^{(i)}$ is a diagonal matrix of complex values that represents the sensitivity map of the i'th coil, C is the number of coils used for data collection, $\mathbf{F} = \text{diag}(F, F, \ldots, F)$ is a block-diagonal matrix that applies the FFT to each $S^{(i)}x$ product, $\mathbf{M} = \text{diag}(M, M, \ldots, M)$ is a block-diagonal matrix, M represents the data sampling mask, and $\mathbf{b} = (b^{(1)}, b^{(2)}, \ldots, b^{(C)})$ is a block-column matrix with $b^{(i)}$ representing the data collected by the i'th coil. When $\mathbf{MFS}$ is full rank (either invertible or over-determined), then the image is uniquely estimated by solving this equation. Equations of this form can be solved with the conjugate gradient method[12] or LSQR methods.[13]

When a single coil is used, one reconstructs an image using compressed sensing by solving equations of the form

$$\underset{z}{\text{minimize}} \ (1/2)\|MF\Psi^* z - b\|_2^2 + \lambda\|z\|_1, \tag{2}$$

where Ψ is the sparsifying transformation, Ψ^* is its adjoint, and $\lambda > 0$ is a regularization parameter. Note that Ψ^* need not be invertible; it can represent an overcomplete basis (e.g., consisting of the wavelet and curvelet transformations). When $A = MF\Psi^*$ satisfies the restricted isometry property in levels, then the solution to Eq. (2) solves the corresponding sparse signal recovery problem.[14,15] Let $z^\star$ be the solution to Eq. (2); then the image is reconstructed with $x^\star = \Psi^* z^\star$.

Sparse SENSE combines model-based reconstruction with compressed sensing;[16] the image is reconstructed by solving the following optimization equation:

$$\underset{x}{\text{minimize}} \ (1/2)\|\mathbf{MFS}x - \mathbf{b}\|_2^2 + \lambda\|\Psi x\|_1.$$

Problems of this form can be solved with the fast iterative shrinkage threshold algorithm (FISTA).[17]

2.2 Model-Based Reconstruction with Compressed Sensing Using Structured Sparsity

Rather than work with the analysis form of the optimization equation used with sparse SENSE,[18,19] we use the related synthesis formulation:[20,21]

$$\underset{z}{\text{minimize}}\ (1/2)\|\mathbf{MFS}\Psi^* z - \mathbf{b}\|_2^2 + \lambda\|z\|_1. \tag{3}$$

This equation can be modified with estimates of the low-pass filtered images as follows:

$$\underset{z}{\text{minimize}}\ (1/2)\|\mathbf{MF}(\mathbf{S}\Psi^* z + \mathbf{x_L}) - \mathbf{b}\|_2^2 + \lambda\|z\|_1, \tag{4}$$

where $\mathbf{x_L}$ is a vector of low-frequency estimates (blurry images) of each coil. Because we do not expect the low frequencies of the image to be sparse, we choose to satisfy the Nyquist–Shannon sampling theorem for the low-frequency portion of the image. The low-frequency, blurry images are estimated with $\mathbf{x_L} = \mathbf{F}^{-1}\mathbf{K_B}\mathbf{M_L}\mathbf{b}$, where $\mathbf{M_L}$ is a block-diagonal matrix of a repeated block M_L with values equal to 1 or 0 that isolates the low frequencies according to the two-level sampling scheme of Ref. 22 and $\mathbf{K_B}$ is a repeated block-diagonal matrix that applies the Kaiser–Bessel window[23] as in Refs. 4 and 5. By letting $\boldsymbol{\beta} = \mathbf{b} - \mathbf{MFx_L} = (I - \mathbf{MK_B}\mathbf{M_L})\mathbf{b}$, Eq. (5) becomes

$$\underset{z}{\text{minimize}}\ (1/2)\|\mathbf{MFS}\Psi^* z - \boldsymbol{\beta}\|_2^2 + \lambda\|z\|_1. \tag{5}$$

Equation (5) is the novel combination of parallel imaging and compressed sensing with structured sparsity. Note that this equation is the same form as Eq. (3), with the only difference being that $\mathbf{b}$ is replaced with $\boldsymbol{\beta}$; it too can be solved with FISTA. Let $z^\star$ be the solution to Eq. (5); then the images of all coils are reconstructed according to $\mathbf{x}^\star = \mathbf{x_L} + \mathbf{S}\Psi^* z^\star$. Once the images of all coils are reconstructed, the final image is reconstructed using the method of Roemer et al.[24]

The model-based reconstruction presented in Eq. (5) that combines parallel imaging with compressed sensing using structured sparsity amounts to a three-step process for image reconstruction: (1) estimate the blurry images $\mathbf{x_L}$, (2) estimate the missing details by solving Eq. (5), and (3) combine the reconstructions from all coils into a single image. For this approach, the low-frequency region must be fully sampled.

3 Results

3.1 Experimental Setup

All experiments are from fully sampled data of anatomies that remain still. Fully sampled reconstructions were generated by the method of Roemer et al.[24] Results will be shown for data with a brain, knee, ankle, and shoulder. The fully sampled reconstructions are compared to the reconstructions from retrospectively undersampled data. All data were collected on Cartesian trajectories with two dimensions of phase encodes and one dimension of readout. All processing in this paper was conducted on individual slices. Sensitivity maps were estimated using the method described in Ref. 25. The sampling patterns used were a variable density Poisson disc sampling pattern (without directional variation) created according to Ref. 26; an example is shown in Fig. 1. Unless otherwise stated, the sampling pattern is augmented with a centered fully sampled region (FSR) [Fig. 1(b)]. After inverse Fourier transforming along the readout direction, the data are placed in a k_x, k_y, z hybrid domain where each slice (i.e., individual z locations) is then processed independently. We show results for individual slices from each dataset. Each equation was solved with values of λ equal to 0.0001, 0.0002, ..., 0.001, 0.002, ..., 0.01, 0.02, ..., 0.1, 0.2, ..., 1. Unless otherwise stated, the image that achieves the lowest relative error (RelErr) is reported; RelErr is defined as

$$\text{RelErr} = \frac{\|\text{truth} - k \cdot \text{estimate}\|_2}{\|\text{truth}\|_2}, \tag{6}$$

where the fully sampled reconstruction is the truth and the undersampled reconstruction is the estimate. Note that, because the scaling of the reconstructed image is irrelevant, a scalar k that minimizes the RelErr for each estimate is identified.

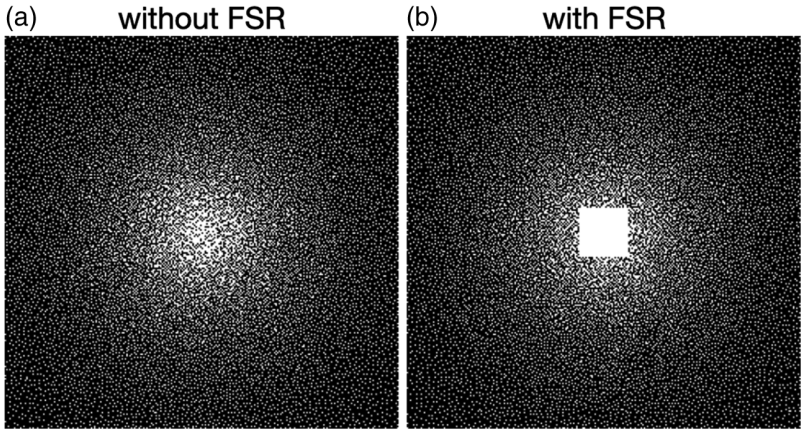

Fig. 1 Variable density Poisson disc sampling patterns (a) without and (b) with an FSR created according to the discrete Daubechies-4 wavelet transform. Each white point represents a line of data from the page that was collected. These sampling patterns create a sampling burden of 24%.

Results from parallel imaging with compressed sensing using structured sparsity are compared with results from sparse SENSE[16] and L1 ESPIRiT.[27]

3.2 Results with Retrospective Downsampling

Figure 2 shows a comparison between the fully sampled reconstruction, sparse SENSE, and parallel imaging with compressed sensing using structured sparsity for data of a sagittal slice of an ankle collected with an eight-channel dedicated ankle coil array. The sampling pattern had an acceleration factor of 6.25 (i.e., only 16% of the number of samples required to satisfy the Nyquist–Shannon sampling theorem were collected). The discrete Daubechies-4 wavelet transform was used as the sparsifying transformation.[28] The RelErrs comparing the undersampled reconstructions and the fully sampled reconstruction show that structured sparsity (RelErr = 0.096) is more similar to the fully sampled reconstruction than sparse SENSE (RelErr = 0.0147) and L1 ESPIRiT (RelErr = 0.103). The difference images show that the errors

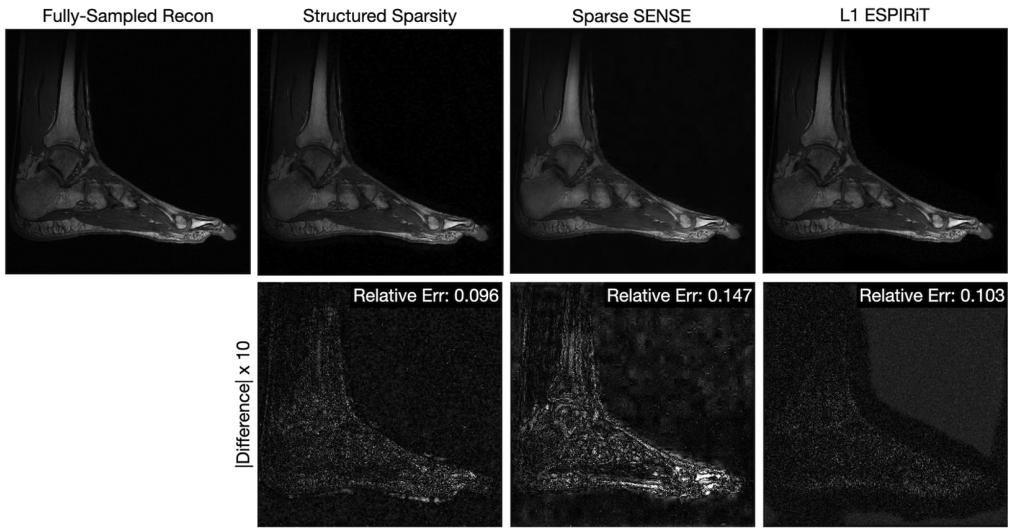

Fig. 2 Comparison of fully sampled reconstruction with reconstructions from undersampled data for a sagittal slice of an ankle with the compressed sensing with structured sparsity presented in this paper and the previously existing sparse SENSE and L1 ESPIRiT. The data collected had an acceleration factor of 6.25. Differences with a fully sampled reconstruction are shown on the same intensity scale. The RelErr is displayed for each reconstruction. Difference images, magnified by 10, are all shown on the same scale.

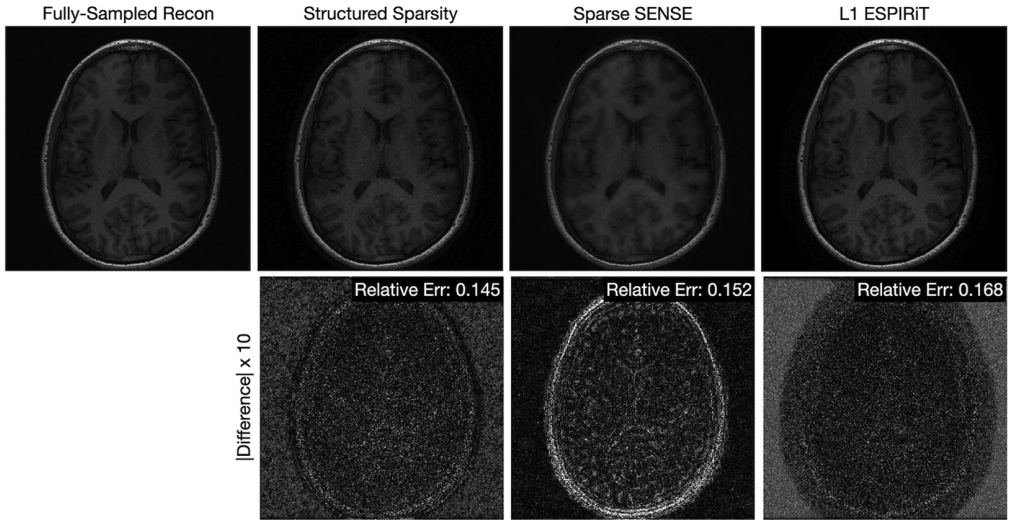

Fig. 3 Comparison of fully sampled reconstruction with reconstructions from undersampled data for an axial slice of a brain with the compressed sensing with structured sparsity presented in this paper and the previously existing sparse SENSE and L1 ESPIRiT. The data collected had an acceleration factor of 5.5. Differences with a fully sampled reconstruction are shown on the same intensity scale. The RelErr is displayed for each reconstruction. Difference images are shown on the same scale.

in sparse SENSE are not isolated to a small region, but are spread throughout the image. Though the details remain visible with sparse SENSE, the low frequencies are highly corrupted.

Figure 3 shows a similar comparison between the fully sampled reconstruction, and reconstructions from 18% of the fully sampled data using parallel imaging with compressed sensing using structured sparsity, sparse SENSE, and L1 ESPIRiT for data of an axial slice of a brain collected with an eight-channel birdcage coil. Again, the Daubechies-4 wavelet transform was used as the sparsifying transformation. As with the ankle, parallel imaging and compressed sensing with structured sampling (RelErr = 0.145) performs better than sparse SENSE (RelErr = 0.152) and L1 ESPIRiT (RelErr = 0.168).

Figure 4 shows a similar comparison between the fully sampled reconstruction and reconstructions from 12% of the fully sampled data using parallel imaging with compressed sensing using structured sparsity, sparse SENSE, and L1 ESPIRiT for data of an axial slice of a shoulder collected with a 16-channel dedicated shoulder array. The sparsifying transform for the structured sparsity and sparse SENSE reconstruction was composed of both the wavelet and curvelet transformations, as in Ref. 5. The top and bottom rows show the full image and an enlarged region, respectively. As with the ankle and shoulder, compressed sensing with structured sparsity attains a better RelErr than compressed sensing alone.

In addition to the ankle, brain, and shoulder data presented in this paper, we determined the RelErr on six other images: two sagittal slices of two different knees using data from Ref. 29, axial slices for the 8-channel and 32-channel brain data shared with Ref. 27, and three axial slices of a brain for data collected by the authors. Table 1 shows the P values that result from a two-sided Wilcoxon signed rank test evaluated on the improvements in RelErrs for all images. Specifically, the test was performed on the differences between the RelErrs of parallel imaging with compressed sensing using structured sparsity and each of the other methods (sparse SENSE and L1 ESPIRiT). If there was negligible improvement, then the differences would be centered around zero and the null hypothesis would be valid. Instead, for almost all cases, the null hypothesis was rejected with a low P value, indicating a significant improvement with the use of structured sparsity.

Figure 5 shows reconstructions for an axial slice of a brain for a variety of different sampling burdens using a sparsifying transformation comprised of wavelets and curvelets. For these images, we report the Pearson correlation coefficient (PCC).[30] For this data, the more significant improvement is achieved when the FSR is included in the sampling pattern; a more minor

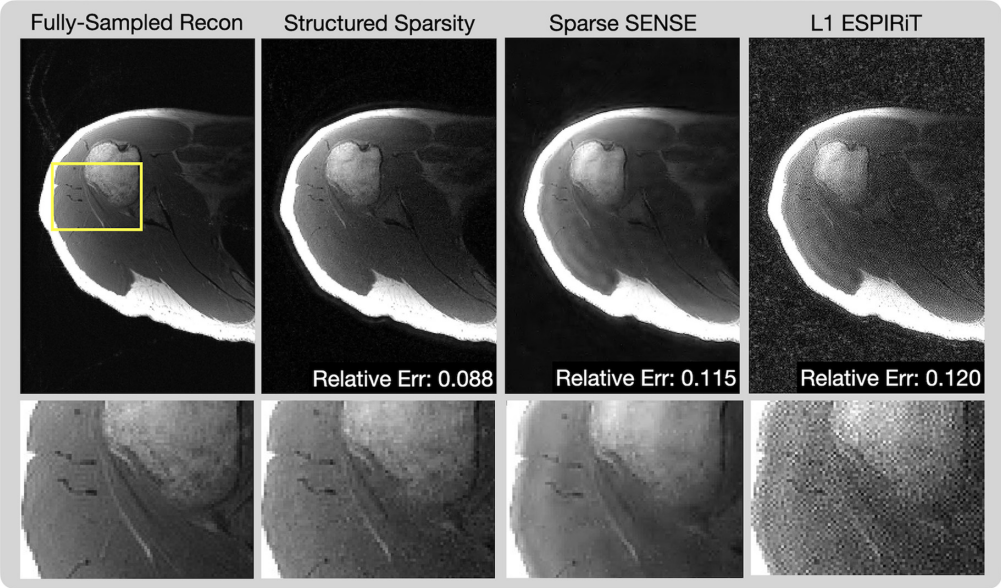

Fig. 4 Comparison of fully sampled reconstruction with reconstructions from undersampled data for an axial slice of a shoulder with the compressed sensing with structured sparsity presented in this paper and the previously existing sparse SENSE and L1 ESPIRiT. The data collected had an acceleration factor of over eight (a sampling fraction of 12%). The top row shows the image reconstructions; the bottom row shows the region enclosed in the yellow box enlarged for improved understanding of the details.

Table 1 *P* values for rejecting the null hypothesis.

Sample fraction	0.12	0.14	0.16	0.18	0.20	0.22	0.24
Sparse SENSE	0.0039	0.0195	0.0156	0.0273	0.0977	0.1289	0.3008
L1 ESPIRiT	0.0547	0.0391	0.0391	0.0391	0.0391	0.0195	0.0195

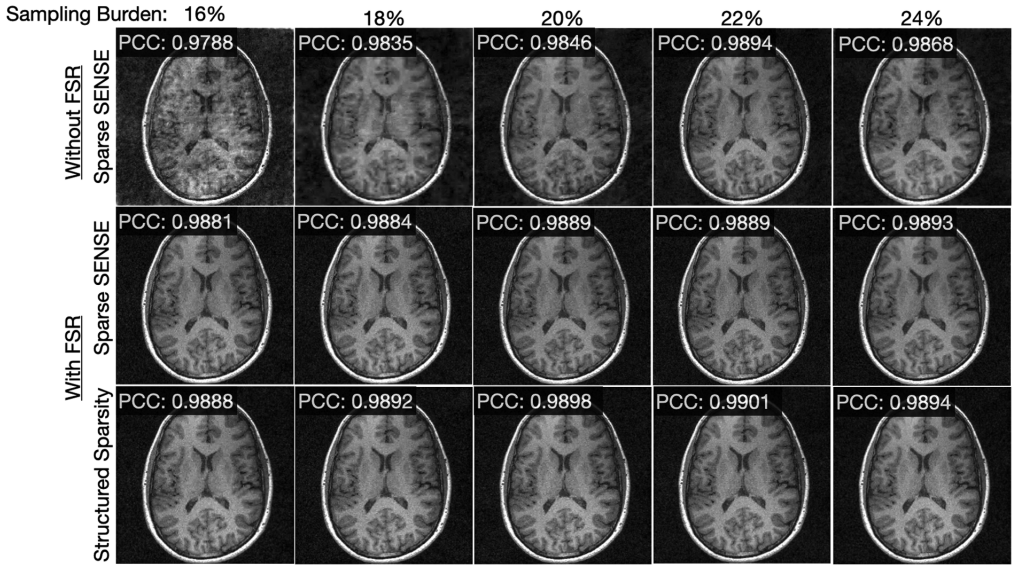

Fig. 5 Reconstructions of an axial slice of a brain. For all sampling burdens, the PCC with structured sparsity is the highest.

improvement is achieved by taking advantage of structured sparsity. This trend is similar to that of compressed sensing using structured sparsity without parallel imaging. In all cases, compressed sensing with structured sparsity outperforms sparse SENSE. Note that compressed sensing with structured sparsity achieves a PCC of 0.9892 with a sampling burden of 18%, which is about what sparse SENSE with the FSR achieves with a sampling burden of 24%. This indicates that one can accelerate the MRI scan by an additional 25% and achieve comparable or better image quality when taking advantage of structured sparsity.

4 Conclusion

When compressed sensing with structured sparsity is combined with parallel imaging, it achieves improved image quality over sparse SENSE (which is compressed sensing and parallel imaging without structured sparsity). The vast majority of the benefit is due to a sampling pattern that includes an FSR, centered on the zero frequency that satisfies the Nyquist–Shannon sampling theorem for the low-frequency bins of the wavelet and curvelet sparsifying transformations. There is a small additional benefit by modifying the optimization problem to take the structured sparsity into account due to the increased sparsity of the resulting optimization variable. This benefit increases as the sampling pattern is reduced, corresponding to a faster MRI scan.

This paper presented compressed sensing with structured sparsity in the context of a model-based reconstruction.[11] Compressed sensing with structured sparsity could also be integrated into parallel imaging based on linear predictability,[31] such as SPIRiT,[32] ESPIRiT,[27] or P-LORAKS.[33] We leave this pursuit as future work.

Disclosures

No conflicts of interest, financial or otherwise, are declared by the authors.

Code and Data Availability

Matlab code used for this project with a sample dataset acquired from mriData.org,[29] which is shared at https://github.com/ndwork/picsWithStructuredSparsity.git. The data of the knee utilized in this study were acquired from mriData.org. Some of the brain data utilized in this study were shared with Ref. 27 and are available at https://people.eecs.berkeley.edu/~mlustig/Software.html. Other data that support the findings of this paper will be made available at www.nicholasdwork.com.

Compliance with Ethical Standards

All procedures performed in studies involving human participants were in accordance with the ethical standards of the Institutional and/or National Research Committee and with the 1964 Helsinki Declaration and its later amendments or comparable ethical standards. MR data of humans were gathered with Institutional Review Board approval and Health Insurance Portability and Accountability Act compliance. Informed consent was obtained from all individual participants included in the study.

References

1. D. K. Sodickson and W. J. Manning, "Simultaneous acquisition of spatial harmonics (SMASH): fast imaging with radiofrequency coil arrays," *Magn. Reson. Med.* **38**(4), 591–603 (1997).
2. A. Deshmane et al., "Parallel MR imaging," *J. Magn. Reson. Imaging* **36**(1), 55–72 (2012).
3. S. S. Vasanawala et al., "Practical parallel imaging compressed sensing MRI: summary of two years of experience in accelerating body MRI of pediatric patients," in *Int. Symp. Biomed. Imaging: From Nano to Macro*, IEEE, pp. 1039–1043 (2011).
4. N. Dwork et al., "Utilizing the wavelet transform's structure in compressed sensing," *Signal, Image Video Process.* **15**, 1407–1414 (2021).
5. N. Dwork and P. E. Larson, "Utilizing the structure of a redundant dictionary comprised of wavelets and curvelets with compressed sensing," *J. Electron. Imaging* **31**(6), 063043 (2022).
6. M. Lustig et al., "Compressed sensing MRI," *Signal Process. Mag.* **25**(2), 72–82 (2008).
7. C. A. Baron et al., "Rapid compressed sensing reconstruction of 3D non-cartesian MRI," *Magn. Reson. Med.* **79**(5), 2685–2692 (2018).

8. J. Ma, "Improved iterative curvelet thresholding for compressed sensing and measurement," *Trans. Instrum. Meas.* **60**(1), 126–136 (2010).
9. G. Beylkin, R. Coifman, and V. Rokhlin, "Fast wavelet transforms and numerical algorithms I," *Commun. Pure Appl. Math.* **44**(2), 141–183 (1991).
10. E. Candes et al., "Fast discrete curvelet transforms," *Multiscale Model. Simul.* **5**(3), 861–899 (2006).
11. J. A. Fessler, "Model-based image reconstruction for MRI," *Signal Process. Mag.* **27**(4), 81–89 (2010).
12. K. P. Pruessmann et al., "Advances in sensitivity encoding with arbitrary *k*-space trajectories," *Magn. Reson. Med.* **46**(4), 638–651 (2001).
13. C. C. Paige and M. A. Saunders, "LSQR: an algorithm for sparse linear equations and sparse least squares," *Trans. Math. Software* **8**(1), 43–71 (1982).
14. D. L. Donoho, M. Elad, and V. N. Temlyakov, "Stable recovery of sparse overcomplete representations in the presence of noise," *Trans. Inf. Theory* **52**(1), 6–18 (2005).
15. A. Bastounis and A. C. Hansen, "On the absence of uniform recovery in many real-world applications of compressed sensing and the restricted isometry property and nullspace property in levels," *J. Imaging Sci.* **10**(1), 335–371 (2017).
16. B. Liu, Y. M. Zou, and L. Ying, "SparseSENSE: application of compressed sensing in parallel MRI," in *Int. Conf. Inf. Technol. and Appl. in Biomed.*, IEEE, pp. 127–130 (2008).
17. A. Beck and M. Teboulle, "A fast iterative shrinkage-thresholding algorithm for linear inverse problems," *J. Imaging Sci.* **2**(1), 183–202 (2009).
18. P. T. Vesanen, F.-H. Lin, and R. J. Ilmoniemi, "Compressed sensing in parallel imaging: towards optimal sampling," in *Proc. Int. Soc. Magn. Reson. Med.*, Vol. 17, pp. 18–24 (2009).
19. L. Feng et al., "Highly accelerated real-time cardiac cine MRI using k-t SPARSE-SENSE," *Magn. Reson. Med.* **70**(1), 64–74 (2013).
20. E. J. Candes et al., "Compressed sensing with coherent and redundant dictionaries," *Appl. Comput. Harmon. Anal.* **31**(1), 59–73 (2011).
21. C. Boyer et al., "Compressed sensing and the synthesis formulation," in *SPARS* (2019).
22. B. Adcock et al., "Breaking the coherence barrier: a new theory for compressed sensing," *Forum Math. Sigma* **5**, e4 (2017).
23. J. I. Jackson et al., "Selection of a convolution function for Fourier inversion using gridding (computerised tomography application)," *Trans. Med. Imaging* **10**(3), 473–478 (1991).
24. P. B. Roemer et al., "The NMR phased array," *Magn. Reson. Med.* **16**(2), 192–225 (1990).
25. K. P. Pruessmann et al., "SENSE: sensitivity encoding for fast MRI," *Magn. Reson. Med.* **42**(5), 952–962 (1999).
26. N. Dwork et al., "Fast variable density Poisson-disc sample generation with directional variation for compressed sensing in MRI," *Magn. Reson. Imaging* **77**, 186–193 (2021).
27. M. Uecker et al., "ESPIRiT—an Eigenvalue approach to autocalibrating parallel MRI: where SENSE meets GRAPPA," *Magn. Reson. Med.* **71**(3), 990–1001 (2014).
28. A. Majumdar and R. K. Ward, "On the choice of compressed sensing priors and sparsifying transforms for MR image reconstruction: an experimental study," *Signal Process. Image Commun.* **27**(9), 1035–1048 (2012).
29. F. Ong et al., "Mridata.org: an open archive for sharing MRI raw data," in *Proc. Int. Soc. Magn. Reson. Med.*, Vol. 26, No. 1 (2018).
30. J. Benesty, J. Chen, and Y. Huang, "On the importance of the Pearson correlation coefficient in noise reduction," *Trans. Audio, Speech Lang. Process.* **16**(4), 757–765 (2008).
31. J. P. Haldar and K. Setsompop, "Linear predictability in MRI reconstruction: leveraging shift-invariant Fourier structure for faster and better imaging," *Signal Process. Mag.* **37**(1), 69–82 (2020).
32. M. Murphy et al., "Fast ℓ_1-SPIRiT compressed sensing parallel imaging MRI: scalable parallel implementation and clinically feasible runtime," *Trans. Med. Imaging* **31**(6), 1250–1262 (2012).
33. J. P. Haldar and J. Zhuo, "P-LORAKS: low-rank modeling of local *k*-space neighborhoods with parallel imaging data," *Magn. Reson. Med.* **75**(4), 1499–1514 (2016).

Nicholas Dwork is an assistant professor at the University of Colorado—Anschutz Medical Campus with a primary position in the Department of Biomedical Informatics, a secondary position in the Department of Radiology, and an affiliate faculty member of the Department of Applied Mathematics at the University of Colorado Boulder. He received his PhD in electrical engineering from Stanford University in 2019 focused on medical imaging. His research interests include medical imaging reconstruction, quantitation, and fast implementations.

Jeremy W. Gordon is an assistant professor in the Department of Radiology and Biomedical Imaging at the University of California, San Francisco. He received his PhD in medical physics from the University of Wisconsin. His research focuses on magnetic resonance spectroscopic

imaging, with a focus on hyperpolarized agents that provide metabolic information. These methods are applied to prostate cancer research, other cancers, and metabolic diseases.

Erin K. Englund is an assistant professor in the Department of Radiology at the University of Colorado—Anschutz Medical Campus. She is a bioengineer and medical imaging researcher with experience developing and applying novel magnetic resonance imaging (MRI) methods to study dynamic physiologic processes. Her work focuses on MRI pulse sequence design, image acquisition, and analysis.